



Critical Considerations in Power Measurements for the Precise Estimation of Energy Costs in Plasma NO_x Synthesis

Ayman A. Abdelaziz^{1,2} · Yoshiyuki Teramoto¹ · Dae-Yeong Kim³ · Tomohiro Nozaki³ · Hyun-Ha Kim^{1,4}

Received: 2 February 2024 / Accepted: 9 April 2024 / Published online: 9 May 2024

© The Author(s), under exclusive licence to Springer Science+Business Media, LLC, part of Springer Nature 2024

Abstract

The great advantage of plasma technology in harnessing abundant clean energy for electrifying and decentralizing the chemical industry holds the promise of attaining carbon neutrality. Therefore, recent research efforts have been dedicated to reducing the energy costs of plasma processes to facilitate the commercialization of this technology. However, it has been noted an inconsistency in reporting energy costs across the literature resulted from inaccurate estimation of power consumption within the system, leading to the misevaluation of the process, its underlying mechanism, and the significance of critical factors. This study comprehensively addresses these challenges by discussing and refining methods for estimating power consumption in a plasma system. Insights are drawn from our ongoing research in plasma NO_x synthesis, specifically a thorough analysis of the discharge dynamics in a recently developed reactor “high-frequency spark discharge” using a high-speed camera, ICCD camera, and high-performance oscilloscope at various pulse widths of the applied voltage. The investigation revealed the importance of accounting for the post-spark period in the voltage cycle during power estimation, as it demonstrates an influence on NO_x synthesis. Furthermore, the study highlighted and addressed critical errors in power measurement and energy cost estimation in the literature. It is found that a significant error, exceeding $\pm 70\%$, arises from overlooking signals delay in the setup and improper adjustment of oscilloscope functions, particularly channel impedance, data averaging, bandwidth, and sampling rate. This paper serves as a valuable guide towards establishing standardized measurements toward the precise estimation of energy costs in plasma processes.

Keywords Plasma technology · Precise estimation of energy costs · Reliability of power measurements · NO_x synthesis · High-frequency spark discharge

Introduction

Over the last decade, the applications of plasma in sustainable fuel and fertilizer production have emerged as a promising technology to achieve carbon neutrality by 2050 [1, 2]. Plasma can be easily generated in air or various gases at atmospheric pressure by applying a relatively high voltage across a pair of electrodes. Numerous plasma sources and reactors powered by various applied voltage (AC, DC, or pulse) have been developed and are currently being optimized for energy and environmental applications [3–15].

A notable example of plasma's unique application is in nitrogen fixation, specifically in NO_x synthesis from air [5, 7, 16–22]. Nitrogen, a triple-bond molecule, requires high energy for dissociation, and its reaction with oxygen to form NO is not feasible from the thermodynamic point of view [7]. Nonetheless, plasmas can successfully perform this reaction under atmospheric conditions without requiring the addition of external chemicals or forces (such as UV) [7]. Among various plasma types, warm plasma stands out due to its capability to generate a high density of electrons with energies ranging from 1 to 3 eV [9, 23]. This characteristic proves advantageous in industrial applications for three main reasons. Firstly, the high electron density accelerates the rate of reactions, reaching percentage levels of product yield. Secondly, the low electron energy transfers a major fraction of the input energy to vibrational excitations of the treated molecules, facilitating their dissociation. Notably, the increase in vibrational excitations of nitrogen molecules facilitates their reaction with oxygen through the vibrational Zeldovich mechanism, resulting in NO formation. Thirdly, the higher electron density with lower energy increases the rotational excitations of the targeted molecules, which in turn increases the temperature. This high temperature within the plasma channel, up to a certain threshold, is beneficial to the oxidation of the formed NO (forward reactions) and the induction of thermal dissociation of nitrogen molecules. In contrast to conventional chemical methods, the combination of these factors enables the highly endothermic NO_x synthesis in one step [24–28]. Likewise, lightning, a natural form of warm plasma, provides a considerable amount of NO_x in nature (approximately 30 Mt/year).

At the outset of the twentieth century, numerous significant endeavors were made to produce nitrogen oxides using arc discharge in air. Success in transitioning this process to industrial applications followed substantial modifications to the setup by Birkeland and Eyde in the early 1900s. They achieved this by generating a stable and practical form of a long arc with the aid of a powerful electromagnet [29]. Despite being replaced quickly by the efficient Haber-Bosch process (HB) for NH_3 production in 1913 [30], there is a renewed interest in warm plasma for NO_x production due to growing concerns related to energy and environmental issues associated with the HB process [31].

Thus, remarkable efforts have been dedicated by the plasma community for effective NO_x synthesis during the last decade [7, 32–39]. These endeavors have provided valuable insights into the mechanism and key factors of plasma NO_x synthesis that influence energy costs and product selectivity control. As a result of this great progress, the transition of plasma technology application in nitrogen fixation from conceptualization to commercialization is accelerated (e.g., www.nitricity.co, <https://n2applied.com/>, and www.plasmaleap.com). However, upon thorough investigation into the techniques and instruments utilized in the literature, we have observed a lack of critical consideration in power measurements, impacting the reliability of energy cost estimations. Examples of common technical errors found in some works include the use of inappropriate oscilloscopes as well as overlook-

ing the delay time of current and voltage probes. One clear result of these errors is the improper alignment of current with respect to voltage. Consequently, notable discrepancies in reported energy costs were found in published literature, even for the same reactor under the same operating conditions. These discrepancies not only impede the reproducibility of measurements but also have the potential to result in a misassessment of the process and reactor performance. Addressing and clarifying this challenge are essential steps toward advancing the reliability and comparability of energy efficiency measurements within the broader plasma research community [40].

A common approach for the estimation of power in plasma reactors involves integrating the product of voltage and current waveforms, regardless of the applied voltage type (AC, DC, or pulse). Various methodologies and recommendations for accurately analyzing electrical measurements to achieve reliable power estimation for many plasma applications were highlighted sporadically throughout the literature. For instance, techniques for estimating plasma power by either eliminating or minimizing capacitive current in AC and pulsed discharge have been reported [41–43]. Benard et al. also emphasized the importance of using an oscilloscope with a minimum bandwidth of 200 MHz and a higher sampling rate to ensure precision in measuring fast discharge dynamics in DBD [44]. To achieve accurate analysis of nanosecond pulsed discharge, the importance of avoiding time delays between voltage and current signals are pointed out in various publications [41, 45, 46]. A thorough study conducted by Ashpis et al. presented a comparison of techniques for current measurement, shedding light on the intricacies of accurate power estimation [47]. Apparently, the primary challenge in power estimation lies in the accurate measurements of the fast rise and fall times of the discharge (in the tens of nanoseconds range). Therefore, careful data acquisition with high-performance instruments becomes paramount, and certain precautions must be considered for recording of current and voltage to achieve a reliable power measurement- a foundational step in evaluating energy efficiency across laboratories to commercial scales. In light of these challenges, it is of great importance to provide a brief overview of the applied techniques for power estimation and common experimental errors that can affect it in one report, enabling a fair evaluation of reactor performance. This becomes particularly relevant given the burgeoning growth of the plasma community, encompassing diverse disciplines such as physics, chemistry, biology, medicine, and agriculture.

Thus, the primary objective of the present study was to clarify the ambiguity surrounding the estimation of electrical power for performance metrics in warm plasma reactors. To achieve this goal, the popular methods employed in the literature for power estimation were applied and discussed in our reactor, and the discharge was monitored using different techniques. Since the focus of this work was not on optimizing operating conditions for efficient NO_x yield, we presented results for a specific condition where pulse widths of the applied voltage were varied while keeping other parameters constant. Furthermore, we systematically examined potential sources of errors, particularly those arising from the experimental setup. Additionally, we delve into the influence of these errors on the accuracy of the energy cost estimation, presenting technical solutions to overcome these experimental problems and ensure the correct set up of the instrumentation. We believe this article provides valuable insights toward the development of reference standards for measuring and expressing power, providing a foundation for the precise estimation of energy costs in NO_x synthesis and various applications of warm plasma reactors.

Experimental Details

The reactor used in this study is based on high frequency spark discharge, which described in detail in [5, 7] and schematically shown in Fig. 1. Two perforated stainless-steel discs with an approximate diameter of 15 mm and thickness of 5 mm are used as high voltage and ground electrode, respectively. The gap between the two electrodes was fixed at 12 mm. The two discs are inserted inside a quartz tube with a length of 170 mm and an inner diameter of 15 mm and a thickness of 1.5 mm. A high-voltage pulsed power supply (PEKURIS, KJ19-5655-04) with variable voltage, pulse widths (P_w) and frequencies (f) is used. The P_w values in this study refer to scale of the pulse width dial on the power supply. The supplied voltage from this power source exhibits a bipolar waveform, with the discharge characteristics nearly identical during both positive and negative voltages. Consequently, only the positive peaks are presented in this paper for better visibility of the change in the waveforms. The applied voltage was measured using a high-voltage probe (Tektronix P6015A), and the current was measured using two Pearson current monitors (model 110 A and 2877). We prefer to not use a shunt resistance technique to measure the current in the present work due to difficulties in finding a proper resistance to accurately measure the current at higher frequencies and fast rise time [47]. The voltage and current waveforms were recorded using a high-performance digital oscilloscope (Tektronix DPO 7054) with adjustable bandwidth and sampling rate. For comparison purposes, a Suematsu pulse power supply capable of delivering voltage up to +30 kV with a frequency up to 500 Hz was used to generate low frequency spark discharge and pulsed corona discharge. Furthermore, a needles-to-plate configuration ($g=13$ mm and space between the needles=20 mm) was used to generate corona discharge in an experiment to show the influence of some parameters on various plasma reactors. Moreover, several attempts were made to achieve accurate power measurements by continuously improving the current measurement techniques and setup connections and adjustments. Only the crucial parameters and techniques are presented in this paper.

The dynamics of the spark in the reactor was monitored using high speed camera (Photron, FASTCAM SA1.1). The frame rate and exposure time of the camera were adjusted to 20,000 frames per second (fps) and 50 μ s, respectively. Additionally, time-resolved images of the spark discharge over a cycle of the applied voltage were investigated using an intensified charge-coupled device (ICCD, Andor iStar DH334T) camera equipped with a Nikkor-UV105 mm lens. The ICCD camera was synchronized with the power supply, and the camera gate-time was fixed at 10 ns, while the delay time was increased in 1 ns step.

The feed gas to the reactors was 50% of nitrogen (purity > 99.999%) and 50% of oxygen (purity > 99.9999%) at a total flow rate (Q) of 1 L/min, which adjusted by mass flow controllers (MFCs, Kofloc Co, FCC-3000). However, to initiate the discharge in the current setup, we introduced only nitrogen into the reactor and applied voltage suddenly at relatively high frequencies and pulse widths. Following the ignition of the discharge, oxygen is introduced alongside nitrogen, and the pulse width and frequency are subsequently adjusted to attain the desired values [5]. The outlet gas from the reactor was quantitatively analyzed using an on-line Fourier transform infrared spectrometer (FTIR) (PerkinElmer, Spectrum One) equipped with a gas cell with a path length of 0.2 m, which was heated at 70 °C. A time-base software (PerkinElmer) was used for continuous monitoring at 20 s intervals with an accumulation of 1 and a scan speed of 0.2 cm/s. Steady state of FTIR intensity was achieved

within approximately 4 min of operation, as illustrated in Fig. 1(b), which showing the typical temporal behavior of absorbance intensity at a wavenumber of 1900 cm^{-1} corresponding to NO IR absorbance. Hence, the average intensities of the FTIR over approximately 10 min after reaching steady state were calculated and used to measure the NO_x concentration. The concentrations of the NO and NO_2 were determined by calibrating the FTIR absorbance for NO and NO_2 using different concentrations of standard gases balanced with N_2 . The calibration was performed at a flow rate and temperature surrounding the gas cell identical to those used in the experiment. The calibration process was carried out across various concentration ranges, and a linear fitting was applied to each of these ranges, as depicted in Fig. 1(c) for the calibration curves of NO. The energy cost of NO_x production is estimated using Eq. (1) after accounting for the gas contraction due to NO_2 formation.

$$\text{Energy cost (MJmol}^{-1}\text{)} = \frac{P(W) \times 24 (\text{Lmol}^{-1}) \times 60 \times 10^{-4}}{Q_c(\text{L/min}) \times [\text{NO}_x](\%)} \quad (1)$$

Here, P and $[\text{NO}_x]$ are the electrical power and NO_x concentration (summation of $[\text{NO}] + [\text{NO}_2]$), respectively. Notably, Q_c represents the corrected volumetric flow rate accounting for changes resulting from product formation [48].

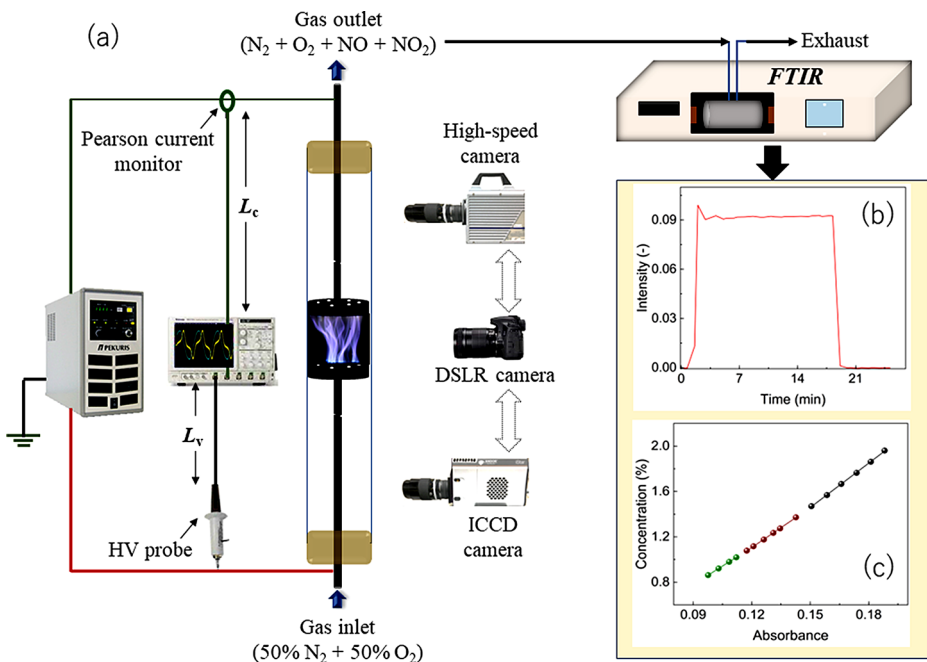


Fig. 1 (a) Schematic of the spark discharge reactor used in the present study. L_V and L_C are the cable length of the HV probe and current monitor, respectively. (b) Intensity of FTIR absorbance at a wavenumber of 1900 cm^{-1} attributed to NO IR absorption (the reactor operated at $P_w=1.8$). (c) Calibration curve of FTIR for NO concentration

Results and Discussion

Clarification of Power Reliability Metrics

Various terminologies have been used in the literature concerning electrical power in plasma systems, including plasma power, power consumed, and input power. The lack of precise definitions and understanding of these terms can lead to incorrect interpretation of results, contributing to misvaluation of reactor performance. To clearly understand and apply these power-related terms correctly, it is imperative to comprehend the power distribution within the system. To ignite discharge in a plasma reactor, high voltage power supply is needed, which amplify and reshape the voltage source (plug voltage) to the required level for the reactor. Each power supply is constructed using electric and electronic components such as resistors, capacitors, coils, diodes, arranged in a circuit to deliver varying shapes of applied voltage (AC, DC, or pulse) with specific specifications. The efficiency of energy transfer from a wall plug to the plasma reactor shows the power loss within the power supply and mismatching between the power supply and reactor [43], predominantly influenced by the electrical circuit and the reliability of electronic components. In RF plasma sources, this efficiency is typically high due to the presence of a matching unit. Advancements in power supply technology have also improved this efficiency to over 85% in various plasma sources [49–51]. However, this efficiency in microwave plasmas is still relatively low. Presenting the difference between plug power and delivered power primarily serves to illustrate the efficiency of the power supply rather than the reactor's performance. While this comparison holds importance for industry, it carries lesser significance for the plasma community. Conversely, the delivered power from the power supply assumes significance in demonstrating the reactor's performance, which is important for both the plasma community and industry. We will name this part of power as total power ($P_{tot.}$), and it is estimated from the applied voltage (V) and current (I) over the entire period of voltage cycle (τ) using Eq. 2.

$$P_{tot.} = f \int_0^{\tau} V \cdot I \, dt \quad (2)$$

By the nature of spark discharge in the present study, the applied voltage drops when the discharge ignites, where the discharge current rises rapidly, reaching a peak of several amperes, as shown in Fig. 2. Notably, the duration of the discharge current is significantly shorter than that of the voltage peak. For instance, when the discharge current width (i.e., discharge period) was about 130 ns, the voltage peak width was about 230 ns. With an increase in the pulse width, the ignition voltage decreased, and it was associated with a lower discharge current with a relatively wider halfwidth, as shown in Fig. 3. The observation of lower ignition voltage at wider pulse widths implies an abundance of residual species, which facilitates the discharge ignition. At the end of the discharge, a ringing voltage emerges, associated with fluctuation in the current, persisting for a relatively wide duration (1–1.5 μ s). This phenomenon is attributed to rapid changes in load impedance after the discharge termination. The amplitude and duration of ringing voltage and current depend on the reactor configuration (e.g., electrode gap and tube diameter) and voltage parameters (e.g., frequency and pulse width). Hereafter, this period of ringing voltage, occurring after the extinction of the spark channel, will be referred to as the post-spark. Fig. 3 demonstrates

Fig. 2 Positive voltage and current waveforms of spark discharge when $g=12$ mm, $f=10$ kHz, and $P_w=2.4$. Inset shows the corresponding instantaneous energy consumed in the reactor

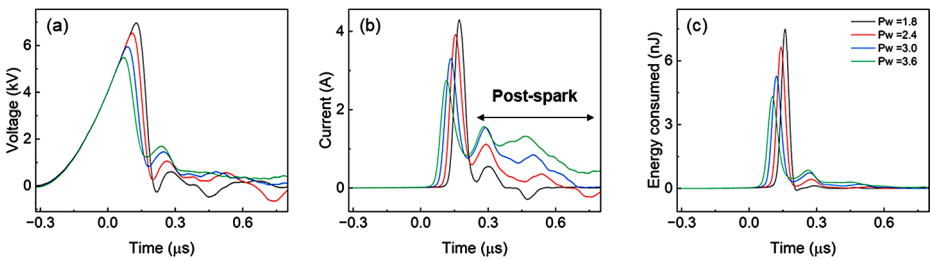
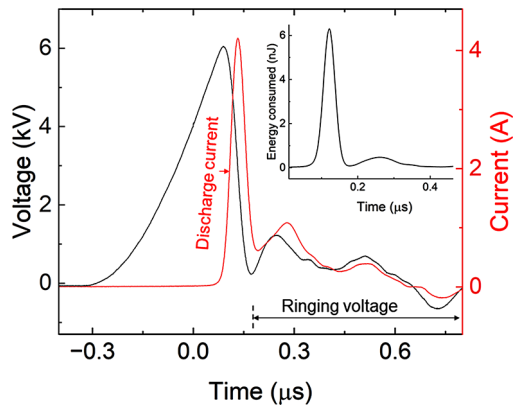


Fig. 3 Influence of pulse width on waveforms of (a) applied voltage, (b) current and (c) energy consumed

the effect of the pulse width on the post-spark duration, where increasing the pulse width intensified the ringing voltage and its corresponding current. The total power, estimated from the entire period of the voltage cycle (including the post-spark period), was about 16.5 W. Meanwhile, the plasma power is determined from Eq. 2 by considering the time of spark period (i.e., the discharge current) rather than the entire period of the discharge current, and it was approximately 12.7 W.

While the dominant power consumption occurs during the discharge current, the contribution of power consumed due to the ringing voltage is noteworthy. As can be seen in Table 1, there is a clear deviation between plasma power and total power reaching more than 40% at a wider pulse width. Furthermore, the trend of increasing the total power with the pulse width is opposite to the trend of the plasma power. Interestingly, NO_x concentration increased with an increase in the pulse width in a similar trend of the total power rather than the estimated plasma power. The strong correlation between NO_x yield and P_{tot} unequivocally demonstrates that P_{tot} is a more reliable metric than plasma power in describing the energy cost in our spark discharge. This correlation also suggests a potential contribution of the post-spark period on the NO_x formation, possibly due to the low E/n during this period, which benefits the process from different perspectives. At low E/n , a significant fraction of energy coupled to the plasma is loaded into molecular vibrational excitations [52], facilitating NO_x formation through the vibrational Zeldovich mechanism. Kunishima et al. [53] reported that applying an external voltage with an E/n below the self-sustaining discharge threshold during high-frequency pulsed discharge enhances the production of nitrogen

vibrational excitation, particularly at wider pulse widths. Additionally, it is expected that the low E/n during the post-spark period affects the behavior of residual charged particles between consecutive discharges. The attachment process of oxygen is known to increase at lower E/n , which can potentially lead to the release of more electrons as the applied voltage increases in next cycle. Therefore, a deeper investigation into the post-spark period for NO_x formation is needed. To this end, it becomes crucial to estimate the energy cost from the total power rather than the plasma power. This approach will facilitate the comparison of various plasma systems and applied operations, enabling a relatively accurate assessment of reactor performance. The maximum NO_x concentration was achieved at a higher pulse width, it was about 1.57% leading to an energy cost of 1.68 MJ/mol (i.e., 78.7 g/kWh) when the total power is considered, and about 1.08 MJ/mol when post-spark period is excluded. This highlights the significant influence of misunderstanding the power definition on the reliability of energy cost estimation, ultimately leading to a misevaluation of the reactor's performance under various operating conditions.

It is worth mentioning that there are other approaches to estimate the plasma power in cold plasma reactors, such as excluding the capacitive current from the total current [41–43], but they are not yet applicable in warm plasma reactors. This is due to the capacitive current in warm plasma reactors and its effect on power estimation is negligible, as we confirmed through our experiments. Consequently, these approaches are not considered in the present study. Furthermore, the discharge power was rarely estimated by narrowing down the entire period of voltage cycle (τ in Eq. 2) to the discharge period detected by the ICCD camera. To gain insights into this technique, we monitored the temporal behavior of the discharge using an ICCD camera with a shorter gate time (10 ns), synchronized with the HV power supply. Apparently, the discharge was clearly observed within a narrow duration of the discharge current corresponding to its halfwidth, as shown in Fig. 4. Additionally, the discharge period detected by the ICCD camera increased with an increase in the pulse width, as indicated in Table 1. After the discharge period, a weak emission of light was observed and diffused even outside the gap, which might be attributed to reflection from the reactor or residual light in the camera due to its relatively high exposure time. The discharge activity at the positive half-cycle is repeated during the negative half-cycle of the applied voltage. However, uncertainty remains in determining the exact discharge period using an ICCD camera because plasma images depend on the camera gain level. Lower gain settings may fail to capture weak discharges, while higher gain settings may result in faulty images, overlapping the brightness of the discharge with the reflected and residual lights in the camera. Therefore, in the present study, the ICCD camera was able to clearly

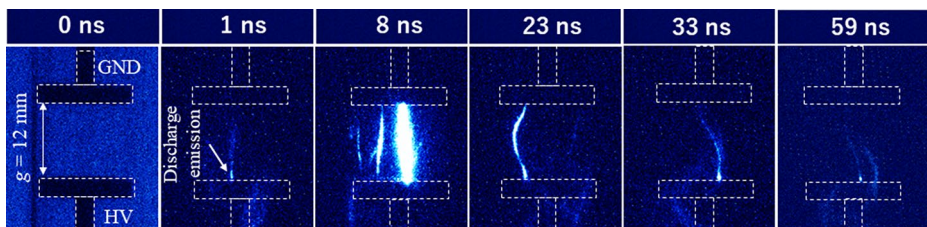


Fig. 4 ICCD images for the spark activity at $g = 12$ mm, $f = 10$ kHz, and $P_w = 2.4$. The ICCD camera synchronized with the high voltage power supply using pulse generator and captured at a gate time of 10 ns. The dashed rectangles in the images are the locations of the HV and ground electrodes

Table 1 Correlation between NO_x concentration and both total power and plasma power, and its effect on energy cost at different pulse widths. The discharge period is the duration of spark illumination as detected by an ICCD

Pulse width	Discharge period (ns)	Total power (W)	Plasma power (W)	NO _x concentration (%)	Energy cost (MJ/mol) ± 0.15	
					using the total power	excluding the post-spark period
3.4	110	18.0	11.6	1.57	1.68	1.08
3.0	90	17.7	12.6	1.52	1.70	1.21
2.4	70	16.5	12.7	1.47	1.65	1.27
1.8	50	13.7	13.0	1.28	1.56	1.48

detect the discharge during the first half of the main current peak only. Consequently, the estimated plasma power derived solely from the ICCD camera observations was found to be half the actual plasma power measured from the current measurements. In contrast, current measurement provides a clearer and more reliable basis for estimating both the total power and plasma power. Therefore, it becomes crucial to clearly describe the applied technique to estimate the plasma power alongside its corresponding equation when presenting data related to power measurements, such as energy cost.

Reliability of Power Measurements

In the preceding section, we refined the definition and estimation techniques of power values in plasma reactors for estimating energy costs. Nevertheless, it's crucial to note that this method's precision is highly rely on the setup arrangement and the characteristics of the measuring instruments. Consequently, in this section, we pinpoint the primary sources of experimental errors to guarantee a relatively high accuracy of power and, subsequently, energy cost estimation.

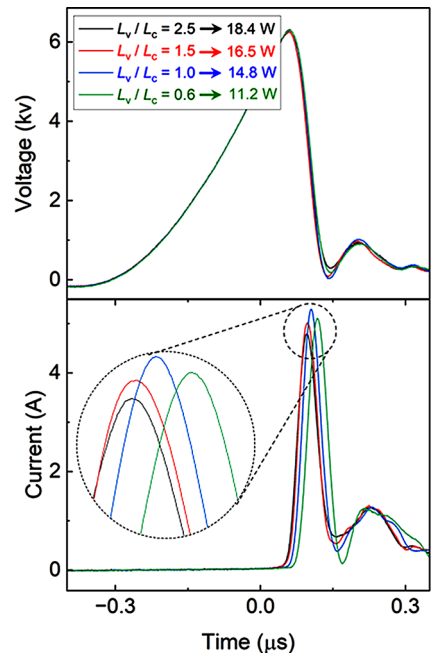
Cable Lengths and Signal Delay

The high voltage delivered to a plasma reactor is measured using a voltage probe, which attenuates the voltage to a measurable level with an oscilloscope. To avoid the effect of noise resulting from the discharge, manufacturers of high voltage probes provided long cables (standard cable lengths are varied in the range of 10 to 30 ft (3.04 to 9.14 m), depending on the manufacturer company) to place the probe at the test reactor while the recording instrument is placed away, in a shielded room for example. On the other hand, current is commonly measured through diverse methods, including current monitors (such as Pearson), Rogowski coil, current probes (for example those provided by Tektronix, Keysight, and LeCroy), or deducing the current from the voltage drop (measured by a low voltage probe) across a resistance. Here, it is important to distinguish between the current monitor (also known as a current transformer with iron core) and the Rogowski coil (without iron core), as numerous publications in the literature have often incorrectly referred to current monitors as Rogowski coils. Certain current probes are equipped with cables of different lengths compared to the HV probe, while other current monitors come without cables and require an external cable. Despite the potential error induced by the signal delay associated

with the varying cable lengths, it has often been overlooked in literature compared to equipment capability. In spark or arc discharge, the discharge period is in the nanosecond range; consequently, a small delay in the current waveform with respect to the voltage waveform can cause a significant effect on the measurement's accuracy.

To verify the influence of signal delay resulting from cables on power measurements, an experiment was carried out using a current monitor connected to an oscilloscope through a cable with varying lengths ($L_c = 1.2, 2.0, 3.0, 5.0$ m), while voltage was measured using a Tektronix high-voltage probe equipped with a standard cable length (L_v) of 3.04 m. The influences of cable length on current and voltage waveforms are illustrated in Fig. 5. Apparently, the current waveform was shifted backwards with an increase in the cable length. For instance, when using a 3.0 m cable for the current monitor, the voltage peak aligns with the start of the current rise (i.e., discharge ignition), consistent with the characteristics of spark discharge. Meanwhile, the voltage dropped after the current rise when $L_v/L_c < 1$, whilst it dropped noticeably before the current rise at current cable lengths shorter than voltage cable length $L_v/L_c > 1$. Consequently, the voltage peak faces a higher current value at longer cable lengths, leading to an overestimation of the power, whereas it aligns with zero current at longer cables, resulting in an underestimation of power. The total power and, subsequently, the energy cost decreases with a decrease in the ratio L_v/L_c , approximately $\pm 12\%$ when there is a ± 1 m difference in the cables of the probes. The energy cost in our previous work [7] was obtained at $L_v/L_c \approx 1.5$; consequently, the corrected energy cost, after accounting for the influence of L_v/L_c , is approximately $\pm 12\%$ lower than the reported value. However, it is important to note that this correction factor ($\pm 12\%$) is affected by both the rise time and width of the applied voltage and current signals. Fig. 6 illustrates the delay time of the current waveform under a different source of the applied voltage (unipolar pulsed voltage) and during a different discharge type, namely pulsed corona discharge. It was found that

Fig. 5 Influence of cable length of probes on current-voltage waveforms at $P_w=2.5$, with fixed cable length of HV probe ($L_v = 3.0$ m) and varied cable lengths ($L_c = 1.2, 2.0, 3.0, 5.0$ m) for the current monitor. The inset provides an enlarged view of current peaks, highlighting the observable delay in the occurrence of the current peak at longer cables



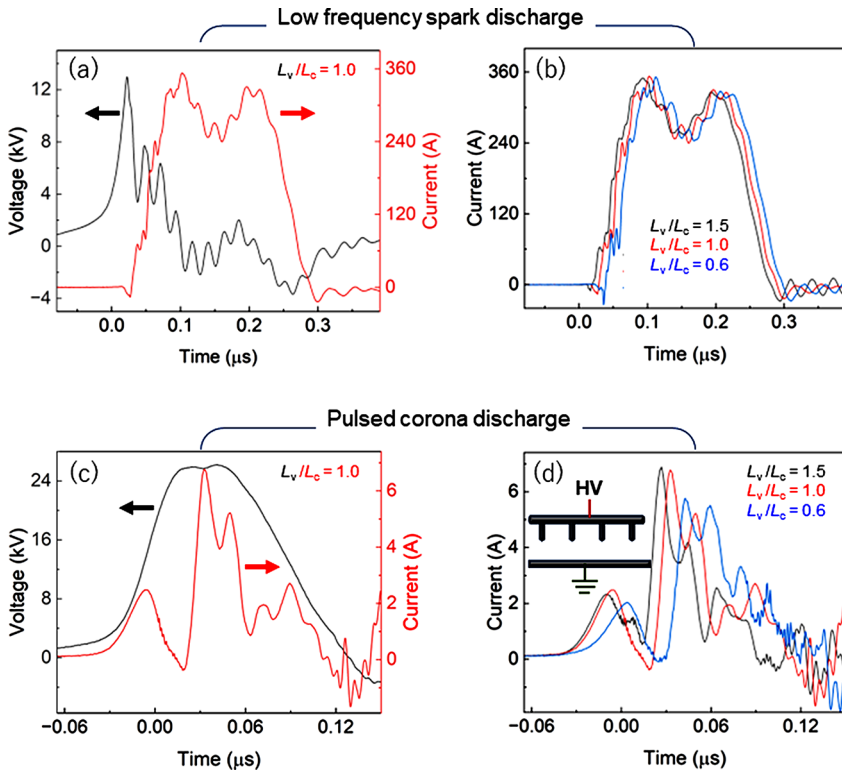


Fig. 6 Effect of cable length on current and voltage waveforms. (a, b) depicts voltage and current waveforms, respectively, of low frequency spark discharge in the main reactor at $g = 5 \text{ mm}$ and $f = 0.4 \text{ kHz}$. (c, d) depicts voltage and current waveforms, respectively, of pulsed corona discharge in needles-to-plate reactor at $f = 20 \text{ Hz}$. $L_c = 2.0, 3.0$ and 5.0 m , while $L_v = 3.0 \text{ m}$. A unipolar pulsed power supply (Suematsu Elect. Co., Ltd., Japan) was used for this set of data

the total power value increased from 115 mW to 126 mW with a decrease in the ratio L_v/L_c from 1.5 to 0.6, respectively. This contrasting trend of power with cable length is attributed to the disparity in discharge ignition among various plasma types. In spark discharge, the voltage drops when the discharge is ignited. Meanwhile, the discharge ignited at a certain voltage and increased with increasing the voltage until its peak in pulsed corona discharge; therefore, the position of current peaks is shifted toward higher voltages. Furthermore, it appears that the increased length of the cable not only caused a time delay but also led to a decrease in current in the low-current pulsed corona discharge, as depicted in Fig. 6 (d), probably due to the weak discharge in this case. Hence, it is imperative to use cables with identical lengths for both the high-voltage probe and current monitors to ensure an accurate estimation of power measurements in plasma reactors.

As mentioned, various methods exist for measuring current in plasma reactors, although they were not utilized in this study. When employing these techniques, it is crucial to consider the delay between the current or low-voltage probes and the HV probe during data processing. An alternative technique for ensuring the accurate temporal alignment of voltage and current in plasma reactors is described in detail in [39, 41]. In this technique, two

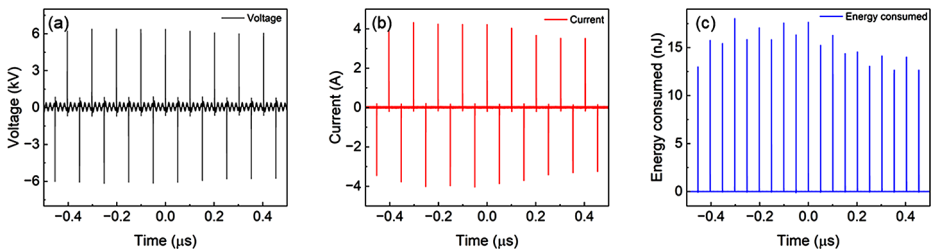


Fig. 7 waveforms of (a) voltage, (b) current and (c) energy consumed of bipolar pulse discharge. The bandwidth and sample rate of the oscilloscope were 500 MHz and 2.5 GS/s, respectively

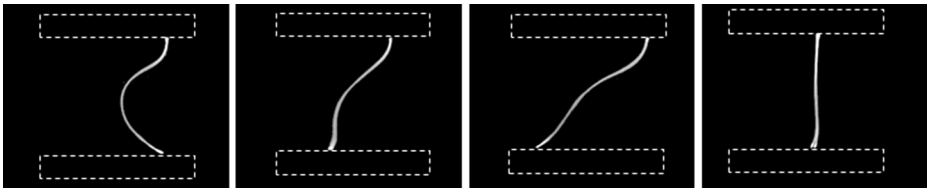


Fig. 8 Typical images show the random spark discharge activity in the reactor. The photos are captured using a high-speed camera with an exposure time of 50 μs . The dashed rectangles in the images are the locations of the HV and ground electrodes

high-voltage probes are connected to opposite ends of a resistor, which is centered inside a current monitor. In this case, the current should rise simultaneously as voltage is applied. Therefore, the offset (deskew) of each high-voltage probe is adjusted on the oscilloscope until alignment is achieved.

Oscilloscope Functions Adjustment

Data Averaging Electrical discharge typically exhibits shot-to-shot variation (i.e., nonuniformity of discharge with time) under fixed conditions in a reactor. Therefore, to get a reliable measurement, adequate averaging of data is highly important and necessary in cold plasma reactors [44]. The nonuniformity of discharge is also pronounced in warm plasma reactors, as shown in Fig. 7 depicting the current and voltage waveforms along with corresponding energy consumption. The data was obtained for an averaging of two for 9.5 cycles of the applied voltage. As can be seen in the figure, there is a notable disparity in the current peaks over time, denoting shot-to-shot variation, significantly reflected in the energy consumed. This nonuniformity in the discharge behavior in warm plasma is evidenced by monitoring the discharge dynamic using a high-speed camera shown in Fig. 8, and it is raised mainly from (1) the roughness in the electrode surface from the strong discharge, (2) the noticeable high temperature associated with the plasma channel and its nonuniform distribution in the reactor that make the discharge takes various pathways, and (3) distribution of residual charges.

The variation in the power consumed in the presented condition (averaging of two of 9.5 cycles) reached 30%. This variation in the power measurements is observed even at higher

cycles of the applied voltage. Therefore, considering an average of a larger number of cycles can ensure stability and reproducibility of power measurement. It is found that an averaging of more than 50 cycles and displaying more cycle waveform are essential for the power measurement in our set-up, and this value should be checked for each plasma reactor. Unless stated elsewhere, we used 62 cycles of the applied voltage for the power measurements in the work presented in this paper.

The Bandwidth and Sampling Rate The bandwidth of an oscilloscope determines its capability to accurately capture and display signals of different frequencies to closely match the actual signal, while the sample rate determines the resolution of an oscilloscope, as it defines the number of samples acquired per second. The shorter the rise time of a signal, the higher the bandwidth of the measuring instruments required ($\text{Bandwidth} = 0.35\text{--}0.5 / \text{rise time}$ [54]). Due to the rapid change of the discharge and fluctuations in current and voltage waveforms, achieving precise measurements requires the use of a high-performance oscilloscope with high bandwidth and sampling rates. This need aligns with the prerequisites for reliable measurement of current in DBD, where a high bandwidth oscilloscope (at least 200 MHz up to 1 GHz) and a high sampling rate (typically a few GS/s) are deemed necessary [44]. Fig. 9 illustrates the influence of oscilloscope bandwidth and sampling rate on the current and voltage waveforms of our high-frequency spark discharge reactor. The current waveform is noticeably influenced by changes in the oscilloscope bandwidth and sample rate, whereas the voltage waveform demonstrates less variation, owing to its slower rise time compared to the current. Lower bandwidth or sampling rates lead to slight deformations in the width as well as the rise and fall times of the current. Moreover, the current waveform exhibits a jagged, zigzag-like shape, at lower 0.05 GS/s. The deformation is not noticed when transitioning from a bandwidth of 500 MHz to 250 MHz, but reducing it further to 20 MHz introduces an error of approximately 20% in power estimation. Remarkably, when both the bandwidth and sample rate are set at low values of 20 MHz and 0.05 GS/s on the oscilloscope, there is a substantial deviation in power estimation, exceeding $\pm 25\%$. Furthermore, data captured at lower bandwidths or sample rates exhibited poor reproducibility, as illustrated by large error bars in Fig. 9 (b) and (d), which can result in an inaccurate estimation of power.

The bandwidth of the probes could also affect the accuracy of the measurements, depending on the characteristics of the applied voltage. In our setup, we compared the results of currents measured using two current monitors with different bandwidths: Pearson 110 A with a bandwidth range of 120 Hz – 20 MHz, and Pearson 2877 with a bandwidth range of 300 Hz – 200 MHz. This comparison was conducted when the two current monitors connected simultaneously in the setup and the oscilloscope bandwidth was fixed at 500 MHz. As depicted in Fig. 10, the probe's bandwidth has minimal effect on the current waveform, with a slight increase in width and a minor decrease in peak when using a higher bandwidth probe. Furthermore, when employing a higher bandwidth probe, the current fluctuations in the post-spark period appear smoother, but this has a negligible influence on power estimation (<5%) due to the low contribution of fluctuated current. Nonetheless, it is recommended to use voltage and current probes with higher bandwidths, particularly when the main current signal contains high frequency components.

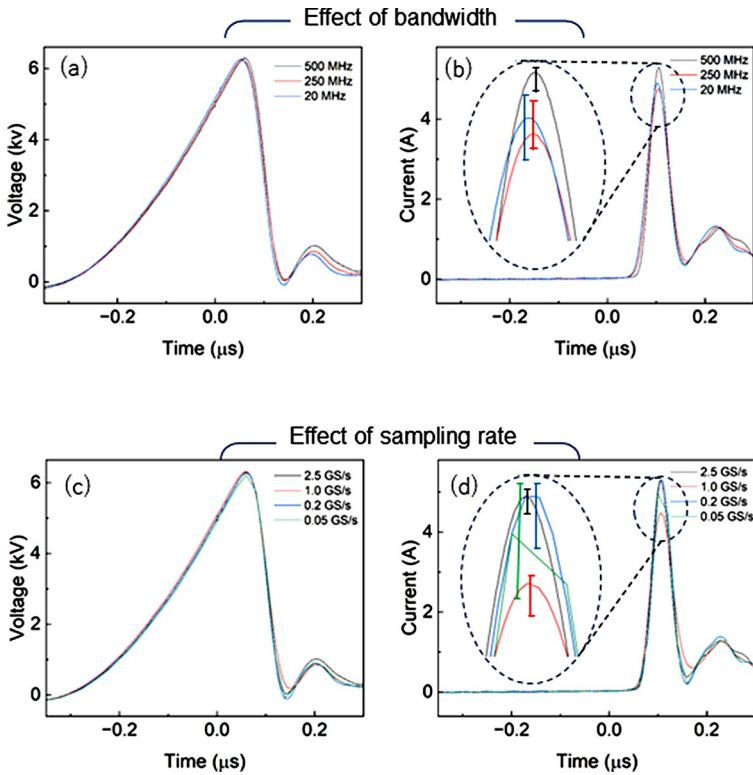
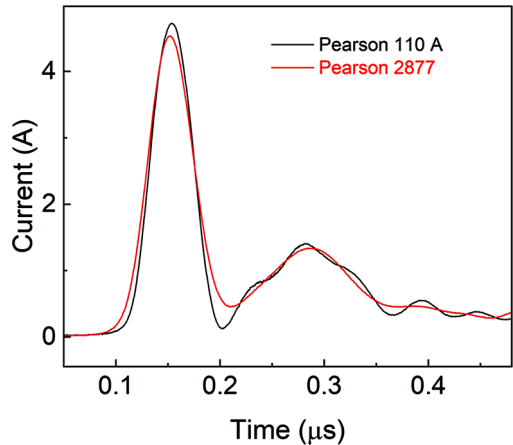


Fig. 9 Influence of oscilloscope bandwidth and sample rate on voltage and current waveforms. (a) and (b) depict voltage and current waveforms, respectively, across different bandwidths while maintaining a constant sample rate of 2.5 GS/s. (c) and (d) voltage and current waveforms at various sample rates with a fixed bandwidth of 500 MHz. Vertical error bars have been added onto the peaks of current signals, revealing significant variations at lower bandwidths or sample rates

Fig. 10 Influence of the bandwidth of current monitors (Pearson 110 A and 2877) on waveform of the current. Bandwidth and sample rate of the oscilloscope was set at 500 MHz and 2.5 GS/s, respectively



Impedance of Oscilloscope Channels and Probes Oscilloscopes manufacturers (such as Tektronix, Keysight, and LeCroy) provided oscilloscopes with a typical input impedance of $1\text{ M}\Omega$, internally connected to each channel. Additionally, high-performance oscilloscopes from these manufacturers offer a selectable function that allows users to change the impedance to $50\ \Omega$. The impedance of the oscilloscope channel must be matched with that of the probes used in the measurements in order to display the waveform correctly without distortion. Commonly, HV probes used in measuring the applied voltage have an impedance of $1\text{ M}\Omega$, which matches the default impedance of the oscilloscope channels. On the other hand, when measuring current using a current monitor (such as the Pearson device utilized in this study), which typically has an impedance of $50\ \Omega$, it is imperative to adjust the channel impedance of the oscilloscope accordingly. However, if the current exceeds the limit value of oscilloscope measurements (usually 5 V in most oscilloscopes) when its impedance is adjusted at $50\ \Omega$, it can potentially damage the oscilloscope. To overcome this problem, a current probe with attenuation (referred to by Pearson as “sensitivity”) of $0.1\text{--}0.01\text{ V/Ampere}$ should be employed, or a $50\ \Omega$ termination adapter should be connected between the oscilloscope channel and the current monitor. Fig. 11 shows how the mismatch between the probe impedance and oscilloscope impedance significantly affects the current measurements. Oscilloscope with $1\text{ M}\Omega$ in its channel give much higher current resulting in overestimation of the power compared to that adjusted at $50\ \Omega$. The power was 30 W in case of $1\text{ M}\Omega$ channel, but it was only 17 W using a channel with $50\ \Omega$ impedance, whilst the NO_x yield remained unaffected. As a result, the energy cost increased by 72% when the channel impedance was not correctly adjusted. It is important to mention that there are coaxial cables with other impedances, such as 75 and $100\ \Omega$. However, to the best of our knowledge, $50\text{-}\Omega$ cable is considered a de facto standard for commercial current monitors. Nevertheless, it is essential to carefully select a cable with an impedance that matches both the current monitor and the impedance of the oscilloscope channel. An improper selection of the cable impedance can lead to impedance mismatching, significantly impacting the accuracy of the measurements due to signal reflection.

Table 2 provides a comprehensive overview of the effect of inadequately adjusted experimental measurements on power estimation within the current reactor. Notably, the table illustrates that the simultaneous misapplication of two or more factors can result in a substantial error in power measurements, consequently affecting the energy cost of the process. Therefore, writing details of experimental setup and instrument functions in published

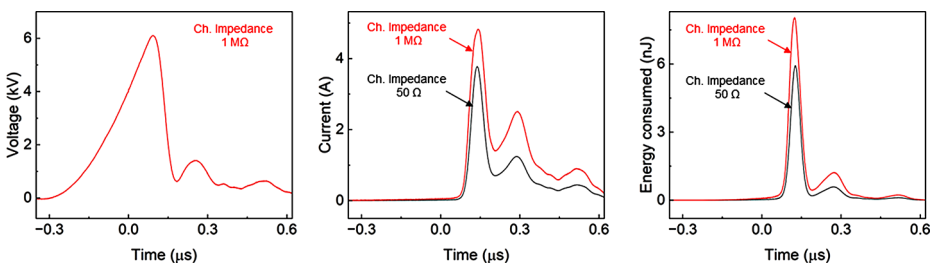


Fig. 11 Influence of adjusting the impedance of oscilloscope channel on (a) voltage, (b) current, and (c) energy consumed. The impedance of the oscilloscope channel for voltage measurements was consistently set at $1\text{ M}\Omega$, while it was varied to either $50\ \Omega$ or $1\text{ M}\Omega$ for current measurements

Table 2 Concise summary of approximate errors arising from inadequate adjustment of experimental measurements

Factor	Approximate error in power estimation
Low data averaging	$\pm 8.0\%$
Delay from 1 m difference in cable length of probes	$\pm 12.0\%$
Bandwidth and sample rate	Up to ± 25.0 , depending on the adjusted value
Incorrect selection of channel impedance of an oscilloscope	72.0%
Estimating the plasma power based on ICCD camera	50%
Difference between plasma power and total power	8–40%, depending on reactor configuration and operational parameters.

papers is necessary to confirm measurement accuracy and facilitate fair comparisons across different works.

Conclusions

In this study, we provided a comprehensive overview of our ongoing efforts to enhance the precision of energy cost evaluations for NO_x production in warm plasma reactors. Analysis of the discharge activity using current-voltage waveforms, high speed imaging and ICCD imaging is performed to give insight into estimation methods of power and eliminate the ambiguity associated with confusing power terminologies in the literature. Experimental evidence suggested that total power (P_{tot}) is a more reliable metric for describing energy costs than plasma power. Additionally, our findings indicate that the post-spark period contributes to NO_x synthesis, yet it has often been overlooked in power estimation in numerous published works. Consequently, there is a pressing need for further research and investigation into this period, particularly in high-frequency discharges.

Furthermore, our deep investigation emphasizes the critical importance of judiciously selecting measuring instruments and making meticulous adjustments. Factors such as cable lengths of the voltage and current probes, as well as improper adjustment of oscilloscope functions including channel impedance, bandwidth, and sampling rate, can significantly impact accuracy and result in remarkable misestimation of power. The degree of inaccuracy worsens when multiple of these factors are involved in experimental measurements. To achieve accurate measurements, researchers must carefully consider the detailed specifications outlined in the datasheets provided by manufacturers for both the probes and oscilloscope, ensuring optimal compatibility and alignment between the measurement tools employed in the setup.

The findings and techniques outlined in this study are particularly pertinent to individuals in the plasma research community and industry, especially those with a chemistry background who may and may not be familiar with the technical challenges involved in measuring plasma characteristics. However, it is essential to link obtained results with studies using various reactors and power supplies to facilitate a comprehensive understanding of the quantitative impact of the discussed factors on the reliability of power measurements.

Acknowledgements This work was supported by JST CREST (grant number: JPMJCR19R3).

Author Contributions Ayman A. Abdelaziz: Conceptualization, Methodology, Data curation, Formal analysis, Investigation, Writing—original draft, Writing – review & editing. Yoshiyuki Teramoto: Investigation, Formal analysis. Dae-Yeong Kim: Investigation, Formal analysis. Tomohiro Nozaki: Formal analysis, Project administration, Funding acquisition. Hyun-Ha Kim: Conceptualization, Investigation, Formal analysis, Writing—original draft, Project administration, Funding acquisition.

Data Availability Data will be made available on request.

Declarations

Competing Interests The authors declare that they have no known competing financial interests or personal relationships that could have appeared to influence the work reported in this paper.

References

1. Zhou R, Zhao Y, Zhou R, Zhang T, Cullen P, Zheng Y et al (2022) Plasma-electrified up-carbonization for low-carbon clean energy. *Carbon Energy* 5(1). <https://doi.org/10.1002/cey2.260>
2. Bogaerts A, Neyts EC (2018) Plasma technology: an emerging technology for energy storage. *ACS Energy Lett* 3(4):1013–1027. <https://doi.org/10.1021/acscenergylett.8b00184>
3. Zhang H, Li L, Li X, Wang W, Yan J, Tu X (2018) Warm plasma activation of CO₂ in a rotating gliding arc discharge reactor. *J CO₂ Util* 27:472–479. <https://doi.org/10.1016/j.jcou.2018.08.020>
4. Sumi N, Sakamoto T, Akimoto Y, Namihira T, Wang D (2023) Conversion of carbon dioxide into carbon monoxide using nanosecond pulsed discharges. *Int J Plasma Environ Sci Technol* 17(1):e01004. <https://doi.org/10.34343/ijpest.2023.17.e01004>
5. Abdelaziz AA, Teramoto Y, Nozaki T, Kim H-H (2023) Performance of high-frequency spark discharge for efficient NO_x production with tunable selectivity. *Chem Eng J* 144182. <https://doi.org/10.1016/j.cej.2023.144182>
6. Winter LR, Chen JG (2021) N₂ fixation by plasma-activated processes. *Joule* 5(2):300–315. <https://doi.org/10.1016/j.joule.2020.11.009>
7. Abdelaziz AA, Teramoto Y, Nozaki T, Kim H-H (2023) Toward reducing the Energy Cost of NO_x Formation in a Spark Discharge Reactor through Pinpointing its mechanism. *ACS Sustain Chem Eng*. <https://doi.org/10.1021/acssuschemeng.2c06535>
8. Wu S, Thapa B, Rivera C, Yuan Y (2021) Nitrate and nitrite fertilizer production from air and water by continuous flow liquid-phase plasma discharge. *J Environ Chem Eng* 9(2). <https://doi.org/10.1016/j.jece.2020.104761>
9. Zhang H, Du C, Wu A, Bo Z, Yan J, Li X (2014) Rotating gliding arc assisted methane decomposition in nitrogen for hydrogen production. *Int J Hydrog Energy* 39(24):12620–12635. <https://doi.org/10.1016/j.ijhydene.2014.06.047>
10. Liu J-L, Li Z, Liu J-H, Li K, Lian H-Y, Li X-S et al (2019) Warm-plasma catalytic reduction of CO₂ with CH₄. *Catal Today* 330:54–60. <https://doi.org/10.1016/j.cattod.2018.05.046>
11. Chen X, Kim HH, Nozaki T (2023) Plasma catalytic technology for CH₄ and CO₂ conversion: a review highlighting fluidized-bed plasma reactor. *Plasma Processes Polym*. <https://doi.org/10.1002/ppap.202200207>
12. Kim H-H, Teramoto Y, Ogata A, Takagi H, Nanba T (2016) Plasma Catalysis for Environmental Treatment and Energy Applications. *Plasma Chem Plasma Process* 36(1):45–72. <https://doi.org/10.1007/s11090-015-9652-7>
13. Diamond J, Profili J, Hamdan A (2019) Characterization of various air plasma discharge modes in contact with Water and their effect on the degradation of reactive dyes. *Plasma Chem Plasma Process* 39(6):1483–1498. <https://doi.org/10.1007/s11090-019-10014-9>
14. Abdelaziz AA, Ishijima T, Tizaoui C (2018) Development and characterization of a wire-plate air bubbling plasma for wastewater treatment using nanosecond pulsed high voltage. *J Appl Phys* 124(5):053302. <https://doi.org/10.1063/1.5037107>

15. Shahidi-Moghadam Z, Ghomi H, Yazdanbakhsh A, Martami M, Rafiee M (2023) Submerged arc plasma treatment of landfill leachate with a high proportion of refractory organics: degradation performance and biodegradability enhancement. *J Environ Chem Eng* 11(6). <https://doi.org/10.1016/j.jece.2023.111330>
16. Pei X, Gidon D, Yang Y-J, Xiong Z, Graves DB (2019) Reducing energy cost of NO production in air plasmas. *Chem Eng J* 362:217–228. <https://doi.org/10.1016/j.ccej.2019.01.011>
17. Rahman M, Cooray V, Montaño R, Liyanage P, Becerra M (2011) NO_x production by impulse sparks in air. *J Electrostat* 69(6):494–500. <https://doi.org/10.1016/j.elstat.2011.06.008>
18. Patil BS, Peeters FJJ, van Rooij GJ, Medrano JA, Gallucci F, Lang J et al (2018) Plasma assisted nitrogen oxide production from air: using pulsed powered gliding arc reactor for a containerized plant. *AIChE J* 64(2):526–537. <https://doi.org/10.1002/aic.15922>
19. Vervloessem E, Aghaei M, Jardali F, Hafezkhiani N, Bogaerts A (2020) Plasma-based N₂ fixation into NO_x: insights from modeling toward optimum yields and energy costs in a gliding arc plasmatron. *ACS Sustain Chem Eng* 8(26):9711–9720. <https://doi.org/10.1021/acssuschemeng.0c01815>
20. Muzammil I, Lee DH, Dinh DK, Kang H, Roh SA, Kim Y-N et al (2021) A novel energy efficient path for nitrogen fixation using a non-thermal arc. *RSC Adv* 11(21):12729–12738. <https://doi.org/10.1039/d1ra01357b>
21. Patil BS, Wang Q, Hessel V, Lang J (2015) Plasma N₂-fixation: 1900–2014. *Catal Today* 256:49–66. <https://doi.org/10.1016/j.cattod.2015.05.005>
22. Janda M, Hensel K, Machala Z, Field TA (2023) The influence of electric circuit parameters on NO_x generation by transient spark discharge. *J Phys D: Appl Phys* 56(48). <https://doi.org/10.1088/1361-6463/ace634>
23. Wang W, Patil B, Heijkers S, Hessel V, Bogaerts A (2017) Nitrogen fixation by gliding Arc plasma: Better Insight by Chemical Kinetics Modelling. *Chemsuschem* 10:2145–2157. <https://doi.org/10.1007/s11090-024-10472-w>
24. Song Y-H, Lee DH, Kim K-T, Kim Y-N, Kang H (2023) Industrial applications of rotating gliding arc plasma. *Int J Plasma Environ Sci Technol* 17:e01005. <https://doi.org/10.34343/ijpest.2023.17.e01005>
25. Lee DH, Kim K-T, Song Y-H, Kang WS, Jo S (2012) Mapping plasma Chemistry in Hydrocarbon Fuel Processing processes. *Plasma Chem Plasma Process* 33(1):249–269. <https://doi.org/10.1007/s11090-012-9407-7>
26. Lee DH, Song Y-H, Kim K-T, Lee J-O (2013) Comparative study of methane activation process by different plasma sources. *Plasma Chem Plasma Process* 33(4):647–661. <https://doi.org/10.1007/s11090-013-9456-6>
27. Snoeckx R, Bogaerts A (2017) Plasma technology - a novel solution for CO₂ conversion? *Chem Soc Rev* 46(19):5805–5863. <https://doi.org/10.1039/c6cs00066e>
28. Kado S, Sekine Y, Nozaki T, Okazaki K (2004) Diagnosis of atmospheric pressure low temperature plasma and application to high efficient methane conversion. *Catal Today* 89(1):47–55. <https://doi.org/10.1016/j.cattod.2003.11.036>
29. Eyde HS (1906) The manufacture of nitrates from the atmosphere by the electric arc-birkeland-eyde process. *J R Soc Arts* 57(2949):568–576
30. Bosch C Process of producing ammonia. In: office Up, editor. US1911
31. Rouwenhorst KHR, Jardali F, Bogaerts A, Lefferts L (2021) From the Birkeland-Eyde process towards energy-efficient plasma-based NO_x synthesis: a techno-economic analysis. *Energy Environ Sci* 14(5):2520–2534. <https://doi.org/10.1039/d0ee03763j>
32. Jardali F, Van Alphen S, Creel J, Ahmadi Eshtehardi H, Axelsson M, Ingels R et al (2021) NO_x production in a rotating gliding arc plasma: potential avenue for sustainable nitrogen fixation. *Green Chem* 23(4):1748–1757. <https://doi.org/10.1039/d0gc03521a>
33. Vervloessem E, Gorbanev Y, Nikiforov A, De Geyter N, Bogaerts A (2022) Sustainable NO_x production from air in pulsed plasma: elucidating the chemistry behind the low energy consumption. *Green Chem* 24(2):916–929. <https://doi.org/10.1039/d1gc02762j>
34. Chen H, Wu A, Mathieu S, Gao P, Li X, Xu BZ et al (2021) Highly efficient nitrogen fixation enabled by an atmospheric pressure rotating gliding arc. *Plasma Process Polym* 18(7):2000200. <https://doi.org/10.1002/ppap.202000200>
35. Britun N, Gamaleev V, Hori M (2021) Evidence of near-the-limit energy cost NO formation in atmospheric spark discharge. *Plasma Sources Sci Technol* 30(8):08lt2. <https://doi.org/10.1088/1361-6595/ac12bf>
36. Dinh DK, Muzammil I, Kang WS, Kim D, Lee DH (2021) Reducing energy cost of in situ nitrogen fixation in water using an arc-DBD combination. *Plasma Sources Sci Technol* 30(5):055020. <https://doi.org/10.1088/1361-6595/abff72>

37. Patil BS, Rovira Palau J, Hessel V, Lang J, Wang Q (2015) Plasma Nitrogen Oxides Synthesis in a millisecond gliding Arc Reactor: investigating the electrical and process parameters. *Plasma Chem Plasma Process* 36(1):241–257. <https://doi.org/10.1007/s11090-015-9671-4>
38. Janda M, Martišovič V, Hensel K, Machala Z (2016) Generation of Antimicrobial NO_x by Atmospheric Air transient spark discharge. *Plasma Chem Plasma Process* 36(3):767–781. <https://doi.org/10.1007/s11090-016-9694-5>
39. Wandell RJ, Wang H, Bulusu RKM, Gallan RO, Locke BR (2019) Formation of Nitrogen Oxides by Nanosecond Pulsed plasma discharges in gas–liquid reactors. *Plasma Chem Plasma Process* 39:643–666. <https://doi.org/10.1007/s11090-019-09981-w>
40. Alves LL, Becker MM, van Dijk J, Gans T, Go DB, Stapelmann K et al (2023) Foundations of plasma standards. *Plasma Sources Sci Technol* 32(2). <https://doi.org/10.1088/1361-6595/acb810>
41. Wang H, Wandell RJ, Locke BR (2018) The influence of carrier gas on plasma properties and hydrogen peroxide production in a nanosecond pulsed plasma discharge generated in a water-film plasma reactor. *J Phys D: Appl Phys* 51(9). <https://doi.org/10.1088/1361-6463/aaa835>
42. Roush RA, Hutcherson RK, Ingram MW, Grothaus MG (1996) Effects of pulse risetime and pulse width on the destruction of toluene and NO_x in a coaxial pulsed corona reactor. *Proceedings of 1996 International Power Modulator Symposium* pp. 79–84
43. Kornev I, Saprykin F, Preis S (2017) Stability and energy efficiency of pulsed corona discharge in treatment of dispersed high-conductivity aqueous solutions. *J Electrostat* 89:42–50. <https://doi.org/10.1016/j.elstat.2017.07.001>
44. Benard N, Moreau E (2014) Electrical and mechanical characteristics of surface AC dielectric barrier discharge plasma actuators applied to airflow control. *Exp Fluids* 55(11). <https://doi.org/10.1007/s00348-014-1846-x>
45. Bulusu RKM, Wandell RJ, Gallan RO, Locke BR (2019) Nitric oxide scavenging of hydroxyl radicals in a nanosecond pulsed plasma discharge gas–liquid reactor. *J Phys D: Appl Phys* 52(50):504002. <https://doi.org/10.1088/1361-6463/ab431a>
46. Gherardi M, Puač N, Marić D, Stancampiano A, Malović G, Colombo V et al (2015) Practical and theoretical considerations on the use of ICCD imaging for the characterization of non-equilibrium plasmas. *Plasma Sources Sci Technol* 24(6). <https://doi.org/10.1088/0963-0252/24/6/064004>
47. Ashpis DE, Laun MC, Griebeler EL (2017) Progress toward Accurate Measurement of Dielectric Barrier Discharge plasma Actuator Power. *AIAA J* 55(7):2254–2268. <https://doi.org/10.2514/1.J055816>
48. Tsonev I, O’Modhrain C, Bogaerts A, Gorbanev Y (2023) Nitrogen fixation by an Arc plasma at elevated pressure to increase the Energy Efficiency and Production Rate of NO_x. *ACS Sustain Chem Eng*. <https://doi.org/10.1021/acssuschemeng.2c06357>
49. Yan K, Hui H, Cui M, Miao J, Wu X, Bao C et al (1998) Corona induced non-thermal plasmas: fundamental study and industrial applications. *J Electrostat* 44(1):17–39. [https://doi.org/10.1016/S0304-3886\(98\)00019-9](https://doi.org/10.1016/S0304-3886(98)00019-9)
50. McAdams R (2007) Pulsed corona treatment of gases: system scaling and efficiency. *Plasma Sources Sci Technol* 16(4):703–710. <https://doi.org/10.1088/0963-0252/16/4/003>
51. Francke KP, Rudolph R, Miessner H (2003) Design and operating characteristics of a simple and Reliable DBD Reactor for Use with Atmospheric Air. *Plasma Chem Plasma Process* 23(1):47–57. <https://doi.org/10.1023/A:1022412718224>
52. Takashima K, Yin Z, Adamovich IV (2012) Measurements and kinetic modeling of energy coupling in volume and surface nanosecond pulse discharges. *Plasma Sources Sci Technol* 22(1). <https://doi.org/10.1088/0963-0252/22/1/015013>
53. Kunishima Y, Takashima K, Kaneko T (2019) Apparent reduced electric field control with nanosecond pulse width in a DC discharge for nitrogen vibrational excitation. *Jpn J Appl Phys* 58(6). <https://doi.org/10.7567/1347-4065/ab1e58>
54. Tektronix (2008) Understanding Oscilloscope Bandwidth, Rise Time and Signal Fidelity. Accessed 2008

Publisher’s Note Springer Nature remains neutral with regard to jurisdictional claims in published maps and institutional affiliations.

Springer Nature or its licensor (e.g. a society or other partner) holds exclusive rights to this article under a publishing agreement with the author(s) or other rightsholder(s); author self-archiving of the accepted manuscript version of this article is solely governed by the terms of such publishing agreement and applicable law.

Authors and Affiliations

Ayman A. Abdelaziz^{1,2} · Yoshiyuki Teramoto¹ · Dae-Yeong Kim³ · Tomohiro Nozaki³ · Hyun-Ha Kim^{1,4}

✉ Ayman A. Abdelaziz
ayman.kotb@aist.go.jp

✉ Hyun-Ha Kim
hyun-ha.kim@aist.go.jp

¹ National Institute of Advanced Industrial Science and Technology (AIST), Environmental Management Research Institute, 16-1 Onogawa, Tsukuba 305-8569, Japan

² Faculty of Science, Assuit University, Assiut 71516, Egypt

³ Department of Mechanical Engineering, Tokyo Institute of Technology, O-Okayama, Tokyo 152-8550, Japan

⁴ National Institute of Advanced Industrial Science and Technology (AIST), Global Zero Emission Research Center, 16-1 Onogawa, Tsukuba 305-8569, Japan